GA–A24223

COMPLETE SUPPRESSION OF THE m=2/n=1 NEOCLASSICAL TEARING MODE USING ELECTRON CYCLOTRON CURRENT DRIVE ON DIII–D

by
C.C. PETTY, R.J. LA HAYE, T.C. LUCE, D.A. HUMPHREYS,
A.W. HYATT, R. PRATER, E.J. STRAIT, M.R. WADE

MARCH 2003

DISCLAIMER

GA–A24223

COMPLETE SUPPRESSION OF THE m=2/n=1 NEOCLASSICAL TEARING MODE USING ELECTRON CYCLOTRON CURRENT DRIVE ON DIII–D

by
C.C. PETTY, R.J. LA HAYE, T.C. LUCE, D.A. HUMPHREYS,
A.W. HYATT, R. PRATER, E.J. STRAIT, M.R. WADE*

This is a preprint of a paper to be submitted for publicaton in *Nucl. Fusion.*

*Oak Ridge National Laboratory, Oak Ridge, Tennessee.

Work supported by
the U.S. Department of Energy under
Contract Nos. DE-AC03-99ER54463 and DE-AC05-00OR22725

GENERAL ATOMICS PROJECT 30033
MARCH 2003

Abstract

The first suppression of the important and deleterious m=2/n=1 neoclassical tearing mode (NTM) is reported using electron cyclotron current drive (ECCD) to replace the "missing" bootstrap current in the island O-point. Experiments on the DIII-D tokamak verify that maximum shrinkage of the m=2/n=1 island occurs when the ECCD location coincides with the q=2 surface. The DIII-D plasma control system is put into "search and suppress" mode to make small changes in the toroidal field to find and lock onto the optimum position, based on real time measurements of dB_θ/dt, for complete m=2/n=1 NTM suppression by ECCD. The requirements on the ECCD for complete island suppression are well modeled by the modified Rutherford equation for the DIII-D plasma conditions.

I. INTRODUCTION

Neoclassical tearing modes (NTMs) are magnetic islands that grow owing to a helical deficit in the bootstrap current that is resonant with the spatial structure of the local magnetic field [1]. The helical loss in bootstrap current is caused by a flattening of the pressure gradient in the O-point (but not the X-point) of the island. The onset of NTMs represent a significant limit to the plasma performance at higher poloidal beta (β_P), where beta is the ratio of the plasma kinetic energy to the magnetic field energy. The $m = 3/n = 2$ mode alone can decrease plasma energy by up to 30% [2]. (Here m is the poloidal mode number and n is the toroidal mode number for tearing modes resonant at safety factor $q = m/n$.) Higher beta values often destabilize the $m = 2/n = 1$ mode which can lock to the wall, rapidly grow and lead to a complete and rapid disruption of the plasma [3]. Control of the $m = 2/n = 1$ tearing mode may be a mandatory element of future high current tokamaks.

The neoclassical tearing mode is particularly well suited to the development of suppression techniques because the mode is linearly stable although nonlinearly unstable, so if the island amplitude can be decreased below a threshold size the mode will decay and vanish. Proposals to stabilize the NTM by the application of local current drive within the magnetic island to mitigate the reduction of the bootstrap current were made by Hegna [4] and Zohm [5]. Electron cyclotron current drive (ECCD) is a particularly promising approach for this purpose because the driven current may be highly localized near the intersection of the electron cyclotron wave with a low order cyclotron resonance. The figure-of-merit for NTM stabilization is the ratio of the current densities at the island location from ECCD and the equilibrium bootstrap current [6]. Thus, if the ECCD is highly localized, then only a small fraction of the total plasma current needs to be driven noninductively to suppress the mode. In addition, while modulating the ECCD to drive current only in the O-point of the island is predicted to be more efficient, using unmodulated ECCD can also suppress NTMs by reducing the island width below the threshold size (assuming the ECCD width is sufficiently narrow) although in principle this requires more gyrotron power than the modulated approach.

Recently several tokamaks have demonstrated the suppression of the $m = 3/n = 2$ NTM using unmodulated ECCD positioned at the island location. On ASDEX Upgrade, co-ECCD was verified to be more effective at NTM stabilization than counter-ECCD or pure heating alone [7–9]. These experiments used a programmed sweep of the toroidal magnetic field to ensure that the current drive layer matched the mode location at some time during the ECCD pulse. On JT-60U, suppression of the $m = 3/n = 2$ mode was also achieved for 1.5 s in steady conditions using ECCD

by optimizing the antenna steering in previous discharges [10]. In both the ASDEX Upgrade and JT-60U experiments, the sawtooth instability that often triggers the NTM was absent. The stabilization of the $m = 3/n = 2$ NTM in the presence of sawteeth was demonstrated for the first time on the DIII-D tokamak [11,12], allowing the plasma beta to be increased above the initial threshold value by $\approx$20% during stabilization of the mode [13,14]. A closed loop feedback scheme was also implemented on DIII-D to match the current drive layer to the mode location by either a rigid radial shift of the plasma or adjustment of the toroidal magnetic field strength [12,15].

In this paper, the first suppression of the more important $m = 2/n = 1$ neoclassical tearing mode is reported, using co-ECCD on DIII-D. The mechanism for the $m = 2/n = 1$ NTM stabilization is the same as for the more benign $m = 3/n = 2$ mode, that is, the replacement of the "missing" bootstrap current by a localized external current drive. However, the $m = 2/n = 1$ NTM is the more difficult mode to suppress because of the stronger mode growth, the less negative tearing stability index (Δ'), and because the $q = 2$ surface is at larger minor radius than the $q = 1.5$ surface (which decreases the ECCD effectiveness owing to the lower electron temperature and increased particle trapping effects [16,17]). The location and magnitude of the ECCD for the $m = 2/n = 1$ NTM suppression is found to be in agreement with theoretical expectations. The ability to suppress this mode opens a significant window for the enhancement of the conventional burning plasma scenario in tokamaks.

The organization of this paper is as follows: in Sec. II, the DIII-D tokamak, plasma conditions, and ECCD system are described. The suppression of the $m = 2/n = 1$ NTM by ECCD is shown in Sec. III, including a discussion of the sensitivity to the ECCD location (Sec. III) and examples of the real-time feedback to find and lock onto the optimum position for complete suppression (Sec. III). The modified Rutherford equation is used to model the requirements on the ECCD for complete island suppression in Sec. IV for comparison with the experiment. The conclusions of this paper are presented in Sec. V.

II. EXPERIMENTAL SETUP

These NTM suppression experiments are done on the DIII-D tokamak [18], parameters for which are major radius $R = 1.67$ m, minor radius $a = 0.6$ m, elongation $\kappa = 1.8$, triangularity $\delta = 0.6$, toroidal magnetic field strength $B_T = 1.4$–1.8 T, and plasma current $I_p = 1.2$ MA. The edge safety factor is typically $q_{95} = 3.8$. The plasma is fueled by deuterium gas puffing and deuterium co-neutral beam injection (NBI), and the vessel walls are boronized to reduce the impurity influx during auxiliary heating. The ELMing (edge localized mode) H-mode discharges utilized in these NTM suppression experiments have several favorable features, including (1) good density control using a divertor cryopump, (2) high electron temperature, (3) quasi-stationary conditions, and (4) the ability to reliably trigger a non-disruptive $m = 2/n = 1$ mode. The first two features are favorable for ECCD, while the last two features allow for a systematic study of NTM suppression methods. The quasi-stationary conditions seem to be a product of a benign $m = 3/n = 2$ tearing mode, steady ELMs (at ≈50Hz), and closed-loop feedback of the density and stored energy using the plasma control system (PCS) [19,20]. This $m = 3/n = 2$ tearing mode has little effect on confinement but apparently is responsible for bringing the current profile into a stationary state without sawteeth or fishbones and with $q(0)$ just above 1. Strong co-NBI keeps the plasma rotating in the presence of the $m = 2/n = 1$ NTM; thus, the mode does not lock to the vessel wall and a disruption is avoided.

Up to five gyrotrons operating at 110 GHz are used in these experiments, with a maximum combined power of 2.7 MW injected into DIII-D [21–23]. The beams are launched from the low field side of the tokamak with a poloidal aiming that can be changed between shots. Each waveguide contains a pair of grooved miter bends that can be oriented to polarize the beam to almost any linear or elliptical polarization [24]. The polarization corresponding to the X-mode dispersion relation is launched in these experiments since it is absorbed strongly for DIII-D conditions. The polarization, propagation, and deposition of the launched electron cyclotron waves have been verified experimentally on DIII-D [25–27]. Figure 1 shows the poloidal cross-section of the DIII-D plasma with the electron cyclotron wave trajectories and the electron cyclotron resonances indicated. The electron cyclotron waves first pass through the third harmonic of the electron cyclotron frequency ($3f_{ce}$) where less than 5% of the power is calculated to be damped before propagating on to the second harmonic resonance ($2f_{ce}$) where the remaining power is absorbed. To drive current at the same location as the $m = 2/n = 1$ NTM, the absorption layer of the electron cyclotron waves should be close to the $q = 2$ surface, which is also indicated in Fig. 1. The aiming of the ECCD antennas is experimentally verified in these experiments

by modulating the beam power and measuring the peak response from a 40 channel electron cyclotron emission (ECE) radiometer[28,29]. The toroidal injection angle for ECCD is chosen to maximize the peak rf current density.

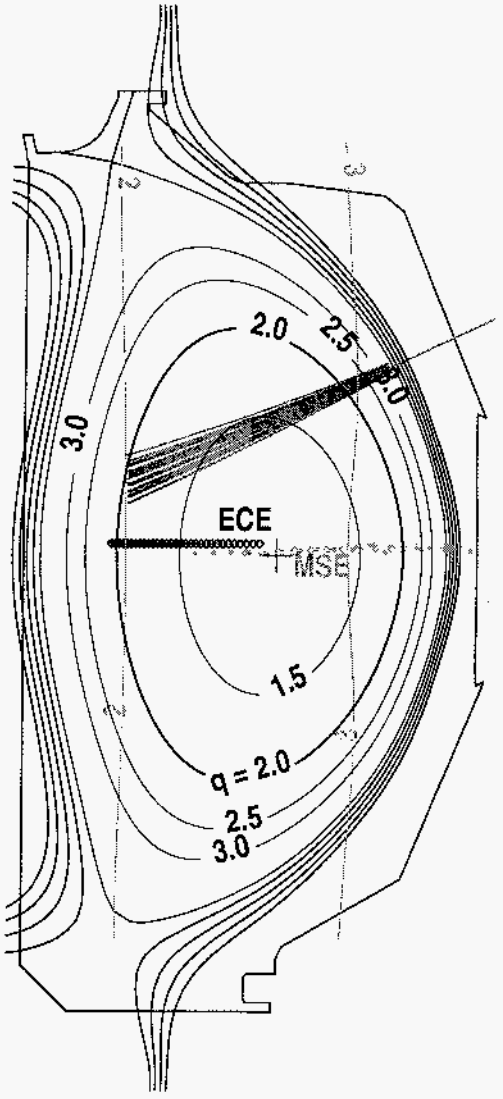

Fig. 1. Configuration for NTM suppression using ECCD showing the q surfaces, 2nd and 3rd harmonic resonance locations, and projection of the electron cyclotron wave trajectories. The locations of the ECE and MSE measurements are also indicated.

III. SUPPRESSION OF THE $M = 2/N = 1$ NTM BY ECCD

A. Sensitivity to ECCD location

Experiments on DIII-D show that the suppression of the $m = 2/n = 1$ NTM is sensitive to the location of the ECCD with regard to the $q = 2$ surface, as expected if the role of ECCD is to replace the "missing" bootstrap current at the island location. The time history of a scan of the ECCD radius and its effect on the $m = 2/n = 1$ NTM amplitude is shown in Fig. 2. The ELMing H-mode discharges used as the target plasmas for these experiments utilize early NBI to slow the plasma current evolution, and contain a benign $m = 3/n = 2$ tearing mode along with closed-loop feedback of the diamagnetic flux using the neutral beams [19,20]. Starting at 3.5 s in Fig. 2, the feedback request on the diamagnetic flux is raised, as seen by the increase in NBI power (P_{NB}) and normalized beta (β_N). When $\beta_N = \beta/(I_p/aB_T)$ reaches the ideal limit for a plasma without a conducting wall [30] ($\approx 4\ell_i$, where ℓ_i is the internal inductance), Fig. 2 shows that a $m = 2/n = 1$ tearing mode is triggered. The onset mechanism for the $m = 2/n = 1$ tearing mode is believed to be related to the approach of ideal stability boundaries and the occurance of poles in the tearing stability index (Δ') [31]. While the initial island may in fact come from the positive Δ' instability, subsequently the growing mode appears to transition into the neoclassical phase with Δ' negative. After the onset and detection of the $m = 2/n = 1$ tearing mode, the PCS automatically decreases the target diamagnetic flux for feedback control to avoid driving the mode to a large amplitude (the energy confinement time also decreases with the onset of the $m = 2/n = 1$ mode). Following the start of injection of 2.7 MW of ECCD power (P_{EC}), the magnitude of B_T is ramped downwards to systematically vary the ECCD location.

The amplitude of the measured $m = 2/n = 1$ tearing mode in Fig. 2 reaches a minimum when the ECCD location passes through the island layer. This is shown in Fig. 3, where the normalized radius of the $q = 2$ surface ($\rho_{q=2}$) determined from EFIT [32] and the normalized radius of the ECCD location (ρ_{EC}) determined from the TORAY-GA ray tracing code [33–35] are plotted during the course of the B_T scan. While there are several possible methods of varying the ECCD location relative to that of the island, such as rigid shifts of the plasma position either radially or vertically, variation of the toroidal magnetic field strength is used in these experiments. (Real time control of the ECCD antenna steering is not currently available on DIII-D but is

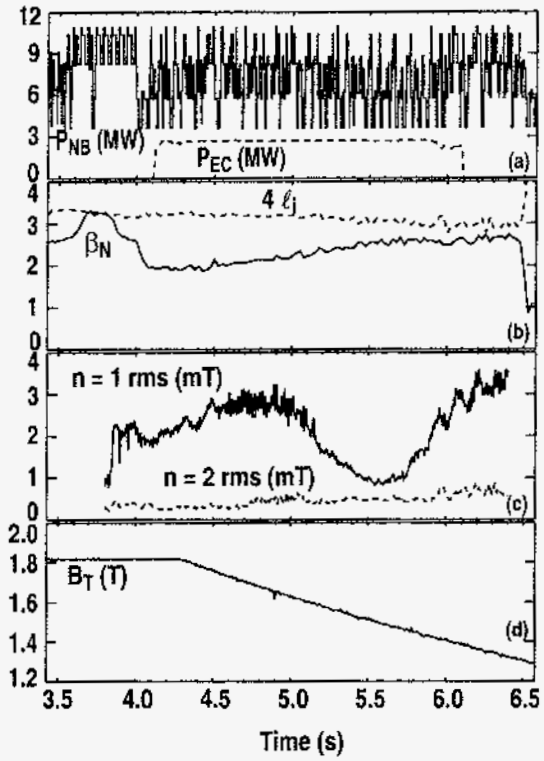

Fig. 2. Time history of discharge #111338 showing (a) NBI (solid) and ECCD (dashed) powers, (b) normalized beta (solid) and ideal no-wall stability limit (dashed), (c) rms amplitudes of n=1 (solid) and n=2 (dashed) tearing modes measured at the wall, and (d) toroidal magnetic field strength. The strong modulation of the NBI power comes from maintaining the plasma diamagnetic flux at a preprogrammed value.

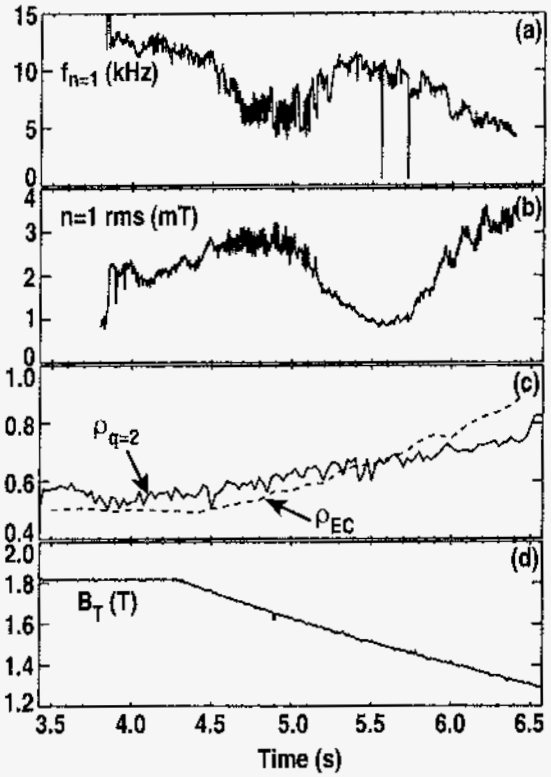

Fig. 3. Time history of discharge #111338 showing (a) rotating frequency of n=1 tearing mode, (b) rms amplitude of n=1 tearing mode measured at the wall, (c) normalized radius of q=2 surface (solid) and ECCD location (dashed), and (d) toroidal magnetic field strength.

planned for the future.) Figure 3 shows that the amplitude of the $m = 2/n = 1$ NTM measured by Mirnov coils outside the plasma reaches a minimum when the ECCD passes through the $q = 2$ surface. The observed minimum in the $m = 2/n = 1$ mode amplitude is independent of the theoretical trend of decreasing ECCD magnitude as B_T is lowered. Figure 3 also shows that the rotation frequency of the $m = 2/n = 1$ island ($f_{n=1}$) peaks around the same time that the island shrinks to its minimum size; the rotation frequency of the $m = 3/n = 2$ island and the toroidal velocity of carbon ions measured by charge exchange recombination (CER) spectroscopy [36] also peak at this time. This peaking of the plasma rotation is compatible with minimizing the drag to induced error currents in the vessel wall in analogy to the induction motor model of external helical fields applied to a rational surface [37,38].

The island structure of the $m = 2/n = 1$ mode is shown in Fig. 4, where the fluctuating electron temperature magnitude ($\propto$ displacement) and phase from the ECE radiometer at the 10 kHz island rotation frequency are plotted as a function of the normalized radius. The measured phase of the ECE fluctuation is observed to shift by $\approx$180 deg around $\rho = 0.66$, which is identified as the location of the island O-point. This is in good agreement with the location at $\rho = 0.67$ of the $q = 2$ surface as determined by the EFIT code. The full width of the island (w), determined from the profile of the ECE fluctuation amplitude, is 11% of the normalized minor radius, or $w = 0.08$ m at the midplane. Figure 4 also shows the radial profile of the flux-surface-average current density from ECCD (J_{EC}) calculated by the TORAY-GA ray tracing code for times before (5.0 s), during (5.5 s), and after (6.0 s) the maximum mode suppression in Fig. 2. It is seen that for ECCD to have an effect on the $m = 2/n = 1$ mode amplitude, the ECCD location needs to be within $\Delta\rho \approx 0.1$ of the island. Furthermore, Fig. 4 shows that the width of the ECCD profile is comparable to the width of the island. In the absence of a NTM threshold, it would be expected theoretically that the ECCD could only reduce the island width to the width of the current drive profile. The fact that the $m = 2/n = 1$ island can be fully suppressed, as shown in the next section, is evidence that the island width only needs to be reduced to a value below the threshold condition, after which the island will decay away.

Further evidence that the ECCD is situated at the island location during the time of peak suppression is given by the motional Stark effect (MSE) data in Fig. 5. Localized ECCD has been demonstrated previously on DIII-D [39,40] from the analysis of changes in the magnetic field pitch angles measured by MSE polarimetry [41]. The magnitude, location, and width of the measured ECCD were found to be in good agreement with theoretical expectations [16,17,42]. This extensive comparison

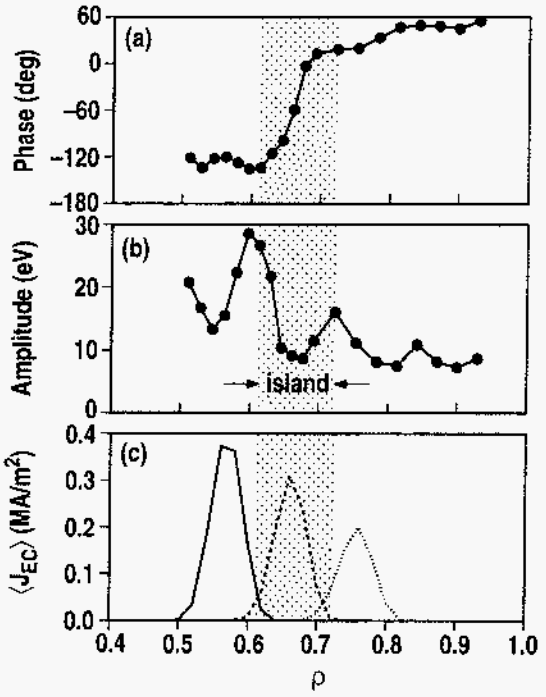

Fig. 4. (a) Phase and (b) rms amplitude of the electron temperature fluctuation measured by ECE at the 10 kHz frequency of the m=2/n=1 NTM as a function of normalized radius. (c) Flux-surface-average current density from ECCD calculated by TORAY-GA for discharge #111338 at times 5.0 s (solid line), 5.5 s (dashed line), and 6.0 s (dotted line). The island location is also indicated.

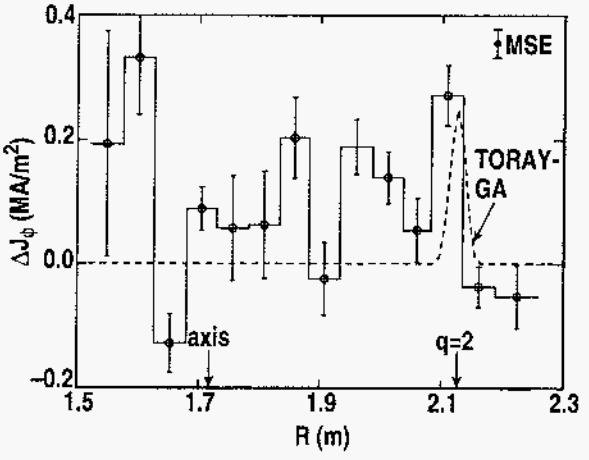

Fig. 5. Change in the toroidal current density (solid line) as a function of major radius, determined from Eq. (1), between discharge #111367 with ECCD and discharge #111335 without ECCD. The plotted rf current density profile (dashed line) is calculated by TORAY-GA. The locations of the plasma axis and q=2 surface are also indicated.

between theory and experiment gives us confidence in using theoretical calculations of ECCD to interpret the NTM suppression results reported in this paper. Figure 5 shows the change in the toroidal current density, as measured by MSE polarimetry, between a discharge with ECCD and a similar discharge without ECCD. The MSE measurement of the vertical component of the magnetic field (B_z) can be related to the toroidal current density (J_ϕ) with an accuracy of 10% for most plasma shapes of interest using the formula [43]

$$\mu_0 J_\phi = -\frac{B_z}{\kappa^2 (R - R_0)} - \frac{\partial B_z}{\partial R} \quad , \tag{1}$$

where R_0 is the major radius of the axis. Figure 5 shows that there is a localized increase in J_ϕ at the major radius where the ECCD is theoretically expected (calculated by TORAY-GA). The location of the $q = 2$ surface from EFIT is also indicated in Fig. 5. Since this analysis is done at the time of maximum mode suppression, Fig. 5 shows that the ECCD is well aligned with the island at this time.

Finally, the plasma performance is observed to peak at the same time the $m = 2/n = 1$ mode amplitude reaches a minimum during the scan of the ECCD location. This is seen in Fig. 6, where the energy confinement time (τ_E) is seen to increase by $\approx 25\%$ when the $m = 2/n = 1$ NTM mode amplitude reaches its minimum value during the ECCD location scan. The energy confinement time then drops by the same 25% when the ECCD position is moved away from the island location. The plasma performance figure-of-merit $\beta_N H_{89}$ is also seen to peak at the same time as the maximum mode suppression, where H_{89} is the measured energy confinement time normalized to an empirical scaling relation for L-mode plasmas [44]. The performance figure-of-merit reaches a value of $\beta_N H_{89} \approx 5$ at the time of maximum mode suppression, which is nearly the same level of performance as the plasma achieved before the onset of the $m = 2/n = 1$ NTM (albeit at a reduced value of B_T).

B. Complete suppression of $m = 2/n = 1$ NTM by ECCD

By carefully controlling the conditions to maximize the effectiveness of the available gyrotron power on DIII-D, complete suppression of the $m = 2/n = 1$ NTM has been achieved for the first time using ECCD to replace the "missing" bootstrap current at the $q = 2$ surface. An example of this is shown in Fig. 7. From 3.2 s to 4.1 s, the value of B_T is ramped down to be close to the optimal value for mode suppression by ECCD as determined from the B_T scans discussed in the previous section.

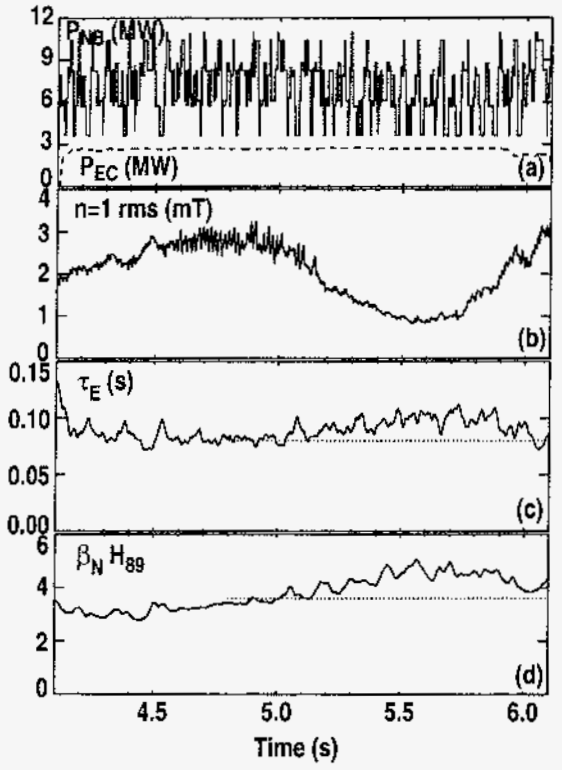

Fig. 6. Time history of discharge #111338 showing (a) NBI (solid) and ECCD (dashed) powers, (b) rms amplitude of n=1 tearing mode measured at the wall, (c) energy confinement time, and (d) performance figure-of-merit product of normalized beta and normalized confinement time.

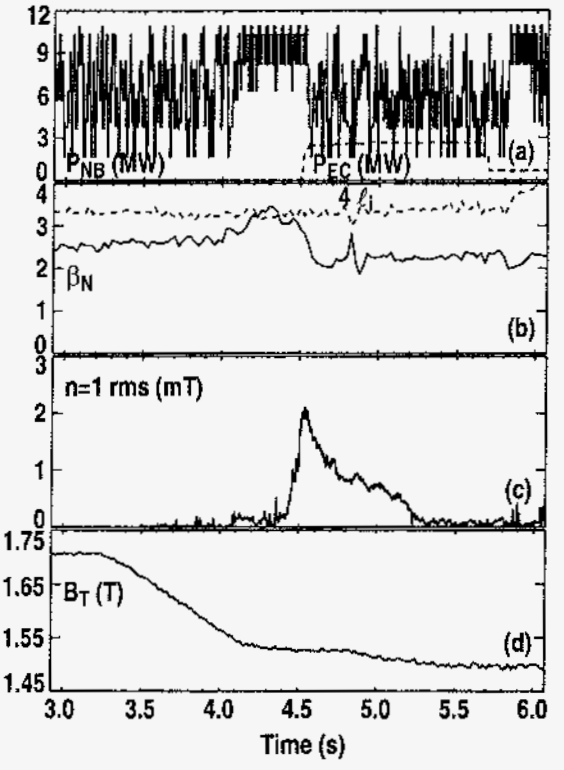

Fig. 7. Time history of discharge #111366 showing (a) NBI (solid) and ECCD (dashed) powers, (b) normalized beta (solid) and ideal no-wall stability limit (dashed), (c) rms amplitude of n=1 tearing mode measured at the wall, and (d) toroidal magnetic field strength.

Soon after the $m = 2/n = 1$ mode starts to grow, 2.7 MW of ECCD is injected into the plasma near the island location at $\rho = 0.66$, driving 40 kA of current according to the CQL3D quasilinear Fokker-Planck code [45] (TORAY-GA predicts nearly the same amount of ECCD). The PCS is then put into a "search and suppress" mode to make small changes in B_T (and, thus, in the ECCD location) to find and lock onto the optimum position for complete island stabilization by ECCD. This is based on real-time measurements of the $m = 2/n = 1$ mode amplitude dB_θ/dt, and is similar to the feedback control method used to suppress the $m = 3/n = 2$ NTM previously on DIII-D [12]. Figure 7 shows that the PCS makes two adjustments to B_T, each of ≈ 0.01 T (equivalent to moving the ECCD location by 0.009 m along the midplane), to find the optimal value, after which the $m = 2/n = 1$ NTM is completely suppressed. The PCS real-time control of B_T is shown in Fig. 8 in more detail, where the time trajectory plot of the $n = 1$ rms amplitude versus B_T is given. After an initial 0.1 s dwell when the ECCD first switches on, the PCS varies B_T by increments of 0.01 T followed by 0.1 s dwells in a "blind search" until the island size drops to zero. At that point, the PCS maintains this B_T value for the duration of the discharge.

A comparison of two discharges, one with complete suppression of the $m = 2/n = 1$ NTM and one without, is given in Fig. 9. The values of the $n = 1$ mode amplitude, line-average density ($\overline{n}_e$), and ECCD power are virtually identical in these two discharges; however, for discharge #111335, the value of B_T is not tuned to the optimal value so that the ECCD location is $\approx$0.10 m away from the optimal position. In these experiments, the NBI power is controlled by PCS feedback to keep the diamagnetic flux at a pre-programmed value, so β_N does not increase when the mode is suppressed. No attempt has been made in these experiments to raise β_N after the stabilization of the $m = 2/n = 1$ mode, although this will be the subject of future work. Note in Fig. 9 that when the requested feedback level of the diamagnetic flux is decreased at 5.8 s for discharge #111335, the amplitude of the $n = 1$ mode decreases but does not disappear. This is consistent with the modeling presented in the next section that shows the $m = 2/n = 1$ mode is robustly unstable for these plasmas, such that without precisely positioned ECCD the tearing mode requires a large decrease in β_N to stabilize by itself.

To completely suppress the $m = 2/n = 1$ NTM in these experiments, it is important to increase the effectiveness of the available ECCD power by operating at the lowest possible density and by steering the separate antennas to drive current at the same radius. The density is kept to a minimum with strong divertor pumping [19,20] and by limiting the particle fueling to that provided by NBI alone. The low density aids ECCD since the driven current is proportional to the power per particle

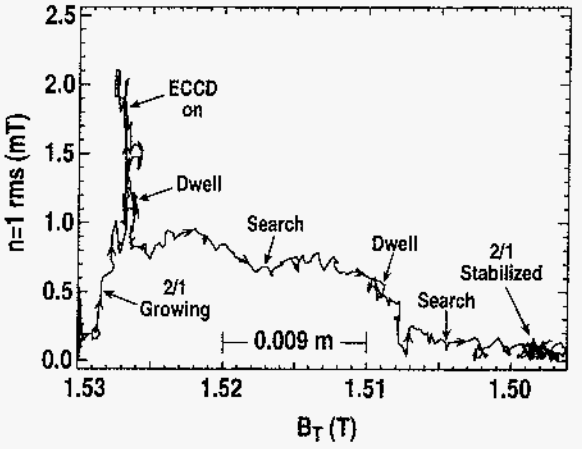

Fig. 8. Trajectory of the rms amplitude of n=1 tearing mode measured at the wall versus the toroidal magnetic field strength with PCS real-time control of the $2f_{ce}$ resonance location for ECCD suppression of an m=2/n=1 NTM (discharge #111366).

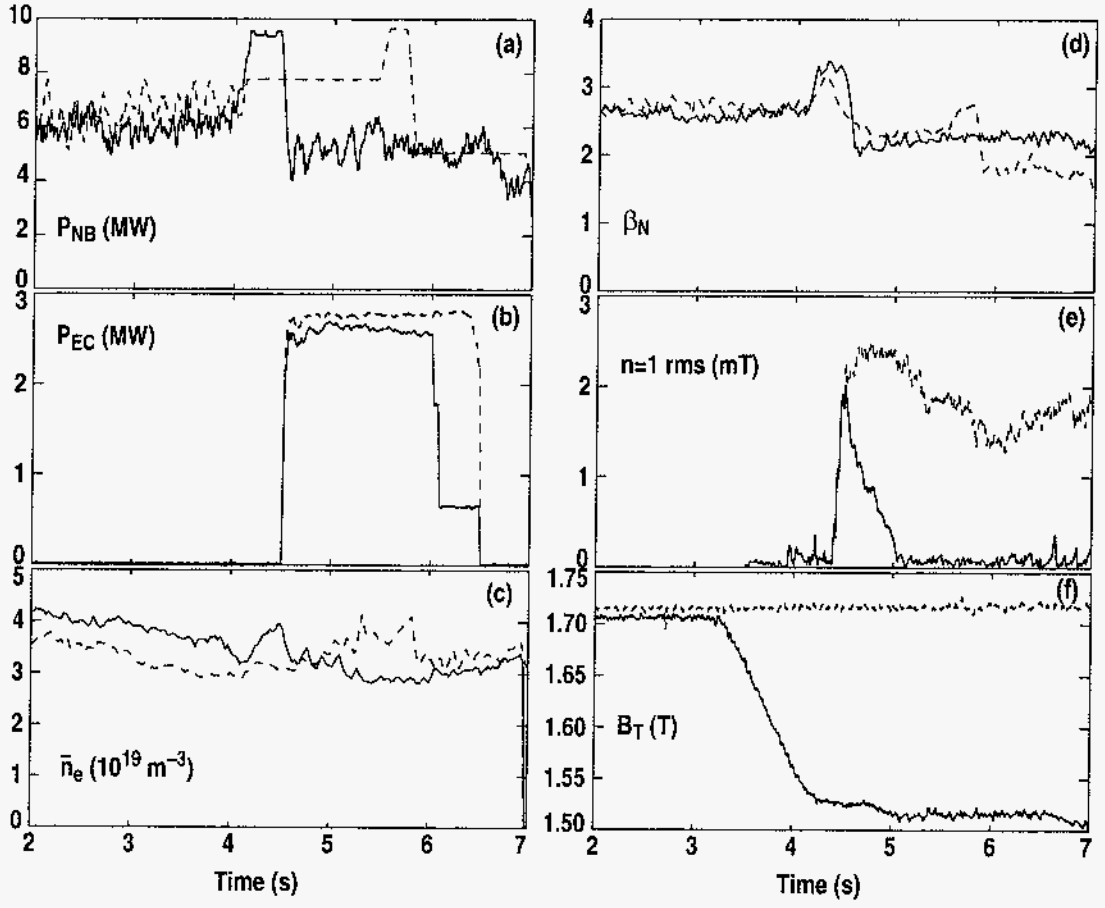

Fig. 9. Time history of discharge #111367 with ECCD on q=2 surface (solid lines) and discharge #111335 with ECCD off q=2 surface (dashed lines) showing (a) NBI power, (b) ECCD power, (c) line-average density, (d) normalized beta, (e) rms amplitude of n=1 tearing mode measured at the wall, and (f) toroidal magnetic field strength.

and also increases with electron temperature. Since five gyrotrons are used in these suppression experiments, it is important to accurately overlap the deposition positions by precise antenna steering to maximize the driven current density at the island location. This is achieved by modulating the gyrotron power and confirming that the peak response in the plasma occurs at the same ECE channel for all of the gyrotrons. Figure 10 shows the radial profiles of the total flux-surface-average current density from an equilibrium reconstruction and the calculated bootstrap (J_{BS}) and ECCD (J_{EC}) current densities. Since the figure-of-merit for NTM suppression is the ratio J_{EC}/J_{BS}), Fig. 10 shows that by aligning all of the gyrotrons it is possible for the local rf current density to exceed that of the bootstrap current density by up to a factor of 2.7 even though the 40 kA of ECCD constitutes only a little more than 3% percent of the total plasma current (compared to 20% for the bootstrap current).

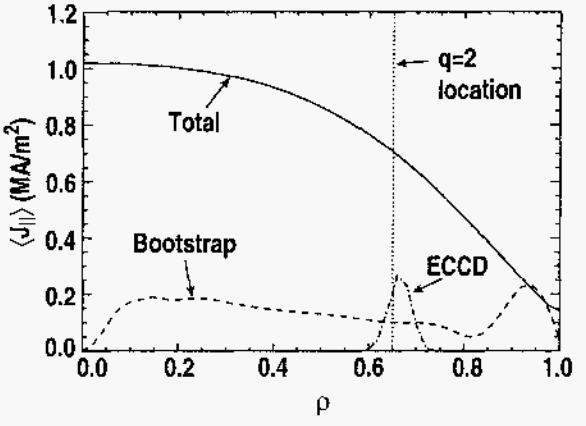

Fig. 10. Flux-surface-average parallel current densities as a function of normalized radius for discharge #111367. The total current density is determined from an equilibrium reconstruction, whereas the bootstrap and ECCD current densities are calculated using the measured plasma profiles. The location of the q=2 surface is also indicated.

IV. THEORETICAL MODELING

The theoretical ratio of the rf current density to the bootstrap current density at the island location required for complete suppression of a NTM can be determined using the modified Rutherford equation [46]. The NTM is metastable since there is a threshold island size above which the island grows large and saturates. Solutions to the modified Rutherford equation, including a term for ECCD as given in Eq. (1) of Ref. [12], are plotted in Fig. 11 for conditions corresponding to $m = 2/n = 1$ NTM suppression experiments on DIII-D with fixed NBI power. Without ECCD, the island has a saturated size of 0.13 m determined from analysis of the Mirnov coils. The modeling displayed in Fig. 11 assumes that the pressure profile peaks as the island shrinks so that the pressure scale length decreases from $L_p = 0.37$ m at $w = 0.13$ m to $L_p = 0.20$ m at $w = 0$. Furthermore, β_p is assumed to increase with shrinking island size, from $\beta_p = 1.2$ at $w = 0.13$ m to $\beta_p = 1.6$ at $w = 0$, since the NBI power is fixed. To fit the measured saturated island width for the no ECCD case, a value of $\Delta' r = -1.25$ needs to be used in the modified Rutherford equation; this value is less negative than for the $m = 3/n = 2$ NTM case on DIII-D [12] making the $m = 2/n = 1$ mode more difficult to suppress. If ECCD is applied with perfect alignment ($\Delta R = 0$) to the island with a peak rf current density of $J_{EC}/J_{BS} = 2.3$, then according to Fig. 11 the island width will shrink to 0.08 m corresponding to a partial stabilization of the tearing mode. This case well models the initial $m = 2/n = 1$ NTM suppression experiments on DIII-D that were only partially successful. The modeling shown in Fig. 11 then predicts that increasing the rf power to give $J_{EC} = 2.8 J_{BS}$ leads to an island growth rate that is negative for any island size; thus, the initially saturated mode amplitude will decrease slowly to about 0.04 m and then rapidly shrink to zero. This ratio of $J_{EC}/J_{BS} = 2.8$ for complete suppression of the $m = 2/n = 1$ NTM is slightly larger than the experimental value of 2.7 shown in Fig. 10, but this is due to the higher value of β_p used in the model. If the actual experimental value of $\beta_p = 0.95$ is used in the modified Rutherford equation, then the theoretical peak rf current density for complete suppression of the tearing mode decreases to $J_{EC}/J_{BS} = 2.3$

As alluded to in the preceeding paragraph, modeling using the modified Rutherford equation shows that the rf current density required for complete NTM suppression decreases with smaller poloidal beta, as shown in Fig. 12. In the complete suppression experiments discussed in Sec. 3, the NBI power is reduced after the $m = 2/n = 1$ NTM onset to avoid driving the mode to large amplitude by limiting the value of β_p. Figure 12 shows a plot of the modeled $m = 2/n = 1$ island width

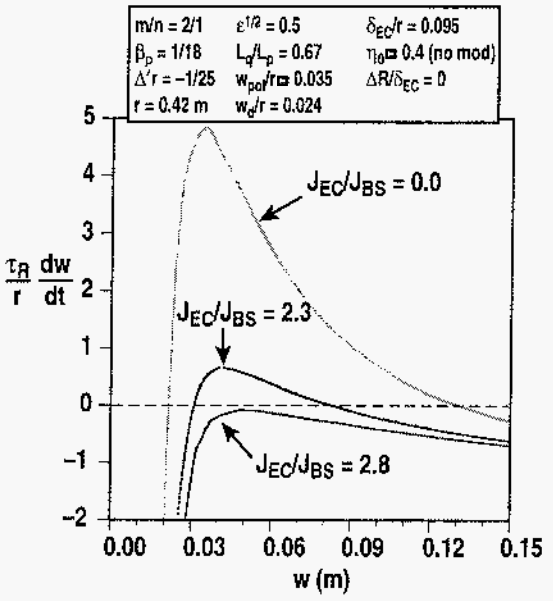

Fig. 11. Island growth rate calculated from the modified Rutherford equation for different levels of precisely aligned rf current density. The model parameters used in Eq. (1) of Ref. [12] for a saturated island width of w=0.13 m are given.

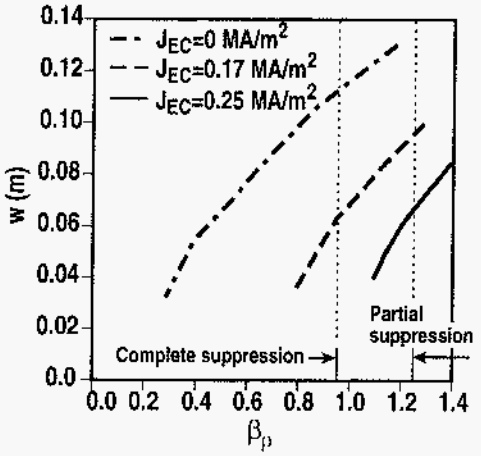

Fig. 12. Calculated width of m=2/n=1 island from the modified Rutherford equation versus poloidal beta for different levels of precisely aligned rf current density. The β_p values for a partial and complete suppression case with J_{EC} = 0.25 MA/m^2 are also indicated (dotted lines).

as a function of β_p for various rf current densities, assuming the ECCD and island are precisely aligned. The pressure scale length is assumed to increase with increasing island size as before. The lowest value of β_p on each curve is the value below which $dw/dt < 0$ for all w, and thus the NTM is stabilized. Without ECCD, the poloidal beta needs to be reduced to $\beta_p = 0.3$ before the $m = 2/n = 1$ NTM vanishes, which is well below the beta values used in these experiments. Applying ECCD with $J_{EC} = 0.17$ MA/m^2 allows stabilization of the $m = 2/n = 1$ mode with higher values of β_p up to 0.8. For the situation corresponding to these DIII-D experiments, $J_{EC} = 0.25$ MA/m^2 should result in NTM stabilization for $\beta_p < 1.1$. The measured β_p values from two discharges on DIII-D are also indicated in Fig. 12. For discharge #107483 with $\beta_p = 1.25$, only a partial suppression of the $m = 2/n = 1$ NTM is observed. However, for discharge #111367 with approximately the same calculated value of J_{EC} but with $\beta_p = 0.95$, complete suppression is obtained. Thus, for a given rf current density (*i.e.*, a given ECCD power), there is an upper limit to the value of β_p for which the $m = 2/n = 1$ NTM can be stabilized.

Finally, the sensitivity of the current drive requirement for complete NTM stabilization to the width of the ECCD radial profile also can be modeled using the modified Rutherford equation. Figure 13 shows a plot of the required ratio of J_{EC}/J_{BS} at the island location for complete suppression of the $m = 2/n = 1$ mode as a function of the full width half maximum (FWHM) of the ECCD profile (δ_{EC}). The integrated ECCD (I_{EC}) normalized to the total plasma current (I_p) is also plotted in this figure. The minimum ratio of J_{EC}/J_{BS} for complete stabilization of the mode occurs at $\delta_{EC} \approx \sqrt{3(w_{pol}^2 + w_d^2)} \approx 0.04$ m (these widths are defined in Ref. [46]), which is the "knee" in the dw/dt versus w curve shown in Fig. 11. This happens to be close to the experimental value of δ_{EC} determined experimentally [12] and is close to the predicted value from the TORAY-GA ray tracing code of $\delta_{EC} = 0.03$ m. Although smaller values of δ_{EC} require higher ratios of J_{EC}/J_{BS} for NTM stabilization, Fig. 13 shows that the total current drive requirement continues to decrease with decreasing δ_{EC}. Since the available gyrotron power is a fundamental experimental limit, narrow ECCD profiles are actually preferred for NTM suppression to reduce the required ECCD and thus the required gyrotron power.

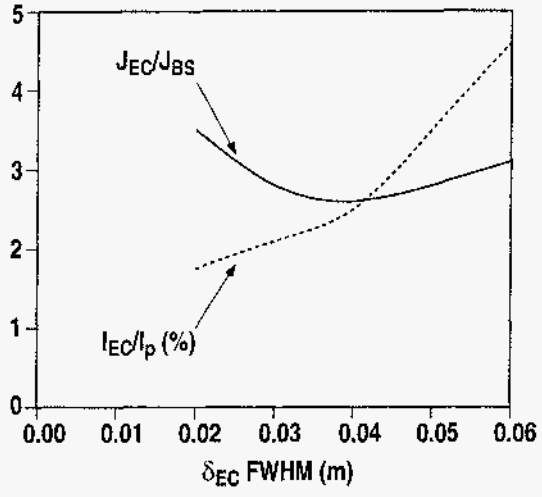

Fig. 13. Required rf current density (solid line) and rf current drive (dashed line) ratios for m=2/n=1 mode stabilization as a function of the ECCD profile width, assuming $\Delta R = 0$ in the modified Rutherford equation.

V. CONCLUSIONS

In this paper, the first suppression of the important $m = 2/n = 1$ neoclassical tearing mode is reported using co-ECCD on the DIII-D tokamak. These experiments use five gyrotrons with 2.7 MW of injected power to drive 40 kA of current at $\rho = 0.66$. By noninductively driving a small fraction of the total plasma current (typically 3%) within the island (located at the $q = 2$ surface), the non-modulated ECCD is able to replace the "missing" bootstrap current and the $m = 2/n = 1$ NTM can be completely suppressed. This stabilization mechanism is similar to that for the $m = 3/n = 2$ NTM, which has been stabilized previously using co-ECCD on several tokamaks [7–12]. The first demonstration of complete suppression of an $m = 2/n = 1$ tearing mode yields confidence that a control system to prevent confinement loss and disruptions arising from this mode can be developed.

These experiments show that the maximum shrinkage of the island size occurs when the ECCD is precisely aligned with the $q = 2$ surface. This is demonstrated by varying the toroidal magnetic field strength to scan the ECCD position in the plasma. A closed loop feedback scheme has been implemented in the plasma control system to actively search for the optimal B_T value for NTM suppression during the ECCD pulse. For conditions of sufficiently localized current drive and not too large poloidal beta, the $m = 2/n = 1$ NTM is fully suppressed in these experiments for the first time. The stabilization of this mode resulted in a $\approx 25\%$ improvement (recovery) of the energy confinement time in these plasmas. The conditions for which complete suppression is obtained ($J_{EC}/J_{BS} = 2.7$) are well modeled by the modified Rutherford equation. The stabilization of the $m = 2/n = 1$ NTM at $\rho = 0.66$ is further evidence for efficient off-axis ECCD with magnitudes in agreement with calculations from the CQL3D quasilinear Fokker-Planck code.

The ELMing H-mode plasmas for these experiments with $q(0) > 1$ owing to a benign $m = 3/n = 2$ tearing mode hold some promise for becoming an alternative high-performance scenario in future burning plasma experiments such as ITER [19,20]. Currently the limit to high performance in these discharges is the onset of the $m = 2/n = 1$ NTM when the beta value exceeds the ideal limit without a conducting wall. Future experiments on DIII-D will attempt to raise the beta value during the $m = 2/n = 1$ stabilization phase with ECCD to determine the new limit to the plasma performance.

REFERENCES

[1] Chang Z. *et al.* 1995 Phys. Rev. Lett. **74** 4663

[2] Günter S., Gude A., Maraschek M., Yu Q. 1999 Plasma Phys. Control. Fusion **41** 767

[3] La Haye R.J., Lao L.L., Strait E.J., Taylor T.S. 1997 Nucl. Fusion **37** 397

[4] Hegna C.C., Callen J.D. 1997 Phys. Plasmas **4** 2940

[5] Zohm H. 1997 Phys. Plasmas **4** 3433

[6] Perkins F.W., Harvey R.W., Makowski M.A., Rosenbluth M.N. 1997 *Proc. 24th Euro. Conf. on Controlled Fusion and Plasma Physics (Berchtesgaden, 1997)* vol 21A (part III) (Geneva: EPS) p 1017

[7] Gantenbein G. *et al* 2000 Phys. Rev. Lett. **85** 1242

[8] Zohm H. *et al* 2001 Nucl. Fusion **41** 197

[9] Zohm H. *et al* 2001 Phys. Plasmas **8** 2009

[10] Isayama A. *et al.* 2000 Plasma Phys. Control. Fusion **42** L37

[11] Prater R. *et al* 2001 Fusion Energy 2000 (Proc. 18th Int. Conf. Sorrento, 2000) (Vienna: IAEA) CD-ROM file EX8/1 and http://www.iaea.org/programmes/ripc/physics/fec2000/html/node1.htm

[12] La Haye R.J. *et al* 2002 Phys. Plasmas **9** 2051

[13] Prater R. *et al* 2002 *Proc. 12th Joint Workshop on Electron Cyclotron Emission and Electron Cyclotron Resonance Heating (Aix-en-Provence, 2002)* to be published

[14] Luce T.C. *et al* 2002 *Proc. 29th Euro. Conf. on Plasma Physics and Controlled Fusion (Montreux, 2002)* vol. 26B (Geneva: EPS) p. P1.059

[15] Luce T.C., La Haye R.J., Humphreys D.A., Petty C.C., Prater R. 2001 *Proc. 14th Top. Conf. on Radiofrequency Power in Plasmas (Oxnard, 2001)* (New York: AIP) p 306

[16] Petty C.C. *et al* 2001 Nucl. Fusion **41** 551

[17] Petty C.C. *et al* 2002 Nucl. Fusion **42** 1365

[18] Luxon J.L. 2002 Nucl. Fusion **42** 614

[19] Wade M.R. *et al* 2001 Phys. Plasmas **8** 2208

[20] Luce T.C. *et al* 2001 Nucl. Fusion **41** 1585

[21] Callis R.W. *et al* 1998 *Proc. 20th Symp. on Fusion Technology (Marseille, 1998)* vol 1 (Saint-Paul-Lez-Durance: Association EURATOM-CEA) p 315

[22] Lohr J. *et al* 1998 *Proc. 23rd Int. Conf. on Infrared and Millimeter Waves (Colchester, 1998)* (Colchester: University of Essex) p 269

[23] Lohr J. *et al* 2001 *Proc. 14th Top. Conf. on Radiofrequency Power in Plasmas (Oxnard, 2001)* (New York: AIP) p 314

[24] Doane J. 1992 Int. J. Infrared Millimeter Waves **13** 1727

[25] Petty C.C. *et al* 1999 *Proc. 13th Int. Conf. on Radiofrequency Power in Plasmas (Annapolis, 1999)* (New York: AIP) p 245

[26] Petty C.C. *et al* 2000 *Proc. 4th Int. Conf. on Strong Microwaves in Plasmas (Nizhny Novgorod, 1999)* vol 1 (Nizhny Novgorod: Russian Academy of Sciences) p 41

[27] Petty C.C. *et al* 2001 *Proc. 14th Top. Conf. on Radiofrequency Power in Plasmas (Oxnard, 2001)* (New York: AIP) p 275

[28] Wang Z. *et al* 1995 *Proc. 9th Int. Workshop on Electron Cyclotron Emission and Electron Cyclotron Heating (Borrego Springs, 1995)* (Singapore: World Scientific) p 427

[29] Austin M.E., Lohr J. *Proc. 14th Top. Conf. on High Temperature Plasma Diagnostics (Madison, 2002)* to be published in Rev. Sci. Instrum.

[30] Strait E.J. 1997 Phys. Plasmas **4** 1783

[31] Brennan D.P. *et al* 2002 Phys. Plasmas **9** 2998

[32] Lao L.L. *et al* 1990 Nucl. Fusion **30** 1035

[33] Kritz A.H., Hsuan H., Goldfinger R.C., Batchelor D.B. 1982 *Proc. 3rd Int. Symp. on Heating in Toroidal Plasmas (Grenoble, 1982)* vol II (Brussels: CEC) p 707

[34] Cohen R.H. 1987 Phys. Fluids **30** 2442

[35] Matsuda K. 1989 IEEE Trans. Plasma Sci. **17** 6

[36] Gohil P., Burrell K.H., Groebner R.J., Seraydarian R.P. 1990 Rev. Sci. Instrum. **61** 2949

[37] Nave M.F.F, Wesson J.A. 1990 Nucl. Fusion **12** 2575

[38] Fitzpatrick R. 1998 Phys. Plasmas **5** 3325

[39] Luce T.C. *et al* 1999 Phys. Rev. Lett. **83** 4550

[40] Luce T.C. *et al* 1999 Plasma Phys. Control. Fusion **411** B119

[41] Rice B.W., Burrell K.H., Lao L.L., Lin-Liu Y.R. 1997 Phys. Rev. Lett. **79** 2694

[42] Lao L.L. *et al* 2001 *Proc. 14th Top. Conf. on Radiofrequency Power in Plasmas (Oxnard, 2001)* (New York: AIP) p 310

[43] Petty C.C., Fox W.R., Luce T.C., Makowski M.A., Suzuki T. 2002 Nucl. Fusion **42** 1124

[44] Yushmanov P.N. *et al* 1990 Nucl. Fusion **30** 1999

[45] Harvey R.W., McCoy M.G. 1993 *Proc. IAEA Technical Committee Meeting (Montreal, 1992)* (Vienna: IAEA) p 498

[46] La Haye R.J. *et al* 2000 Phys. Plasmas **7** 3349

ACKNOWLEDGMENTS

This work is supported by the U.S. Department of Energy under Contract Nos. DE-AC03-99ER54463 and DE-AC05-00OR22725. The authors would like to thank M.E. Austin for operating the ECE diagnostic and M.A. Makowski for operating the MSE diagnostic.